ELECTRONIC SUPPLEMENTARY INFORMATION (ESI)

Part I. Sample preparation and analysis

Preliminary solubility tests and "solid phase + liquid phase region" determination

Samples of paracetamol in pyridine mixtures were prepared at paracetamol concentrations of 20, 40, 50, 60, 80 per cent by weight (11.6, 25.9, 34.3, 44.0, 67.7 mol %). Weighed samples of paracetamol (Merck) were added to the calculated quantity of pyridine on stirring at approximately 330 K. In the case of samples with a high paracetamol content (50, 60 and 80 wt. %), heating to 330 K did not result in complete dissolution of paracetamol. The mixture was therefore stirred for several hours at this temperature, after which it was slowly cooled to room temperature (295 K). The resulting mixtures (sealed from atmosphere) were equilibrated at room temperature for several weeks, after which the precipitates, with a small amount of the stock solution, were taken for XRD analysis.

Frozen solution

1.4 g of paracetamol was dissolved on stirring at 330 K in 2.11 g of pyridine. The hot solution was splashed as a thin layer onto a copper plate cooled to 77 K, and transparent pieces of frozen solution were preliminarily separated from the plate manually as described in [S1].

Crystallisation

Samples of frozen paracetamol in pyridine solutions, prepared as described above, were carefully but gently ground in a mortar at 77 K and placed onto a transparent borosilicate glass vial (Sci/Spec, B75525), which was preliminarily cooled to 77 K. Subsequently, the vial was closed tightly with a TFE cap, put onto a massive copper cell and placed in a thermally insulating shell (hereafter "holder") preliminarily cooled to 77 K. The cell was then heated to 230 K at the rate of roughly 2 K/min. The cell was heated from 230 to 260 K at 0.2-0.4 K/min and kept for 3 hours at this temperature. The cell was then cooled to 230 K at a similar rate. The vial, cooled to 230 K, was removed from the holder and placed overnight in an air thermostat at 260 K. The next day the vial was placed into a holder preliminarily cooled to 230 K, at which point it was heated to 260 K at 0.2-0.4 K/min. Remaining steps were performed as described above; 1 or 2 cooling-heating cycles were carried out daily. The vial contents were visually controlled to track changes in the sample`s morphology (from gel-like to small number of single crystals in a stock solution).

Powder X-ray diffraction

The X-ray diffraction study aimed to identify the phases formed on rapid cooling of paracetamol in a pyridine solution (hereafter "frozen solution"). This was performed using synchrotron radiation at the 4th beamline of the VEPP-3 storage ring (Budker Institute of

Nuclear Physics SB RAS), at fixed wavelength of 0.3675 Å [S2]. The Debye-Sherrer scheme was applied. An MAR345 imaging plate detector (pixel dimension 100 μm) was used to record the diffraction pattern. The distance between the sample and the detector (about 370 mm) was calibrated using a finely dispersed NaCl standard (specific surface area: 2.9±0.1m^2/g), prepared by spray-freeze drying aqueous solutions (~ 12 wt. %). The sample of frozen paracetamol in pyridine solution, prepared as described above, was placed into an aluminium cell with the two foam-coated holes for the primary beam and the outlet of diffracted radiation. The cell was heated at approximately 3 K/min, starting from 77 K. Powder diffraction patterns were recorded continuously. Each diffraction pattern was collected for 4 minutes, so that the temperatures corresponding to the start and the end moment of a pattern differed at about 12 K. The temperature corresponding to a pattern was taken as the average temperature over this interval [S3]. Data were integrated using FIT2D [S4].

For X-ray powder diffraction experiments aimed at characterising the final solid product formed by annealing frozen solutions (with subsequent removal of the pyridine by evaporation under reduced pressure and temperatures slightly above the pyridine melting point (~ 230 K)), Bruker D8 Advance (λ=1.5406 Å, tube voltage of 40 kV and tube current of 40 mA) was used, equipped with a low-temperature TTK 450 Anton Paar chamber allowing work under vacuum down to 10^{-3} torr. The sample was carefully, but gently, ground in a mortar at 77 K and placed onto a holder, which was preliminarily cooled to 140 K. Diffraction patterns were measured across temperatures from 140 – 330 K (2Θ scans in the 5-55 degrees range, at a 0.02 degrees step, about 8 minutes per pattern). Two-dimensional XRD patterns of paracetamol-pyridine quench-cooled solutions at different temperatures, illustrating formation of amorphous and crystalline phases in the system are plotted at Figure S1.

Part II. The choice of model of phase diagram

Based on our previous experiments the equilibrium “paracetamol-pyridine” phase diagram was taken to be of the eutectic type, without formation of any intermediates.

We have started with the following initial assumptions, which seemed reasonable:

1) Only one solvate (with a hypothetical constant stoichiometry of 1:2; 1:1; or 1:0.5) could be formed, but not a solid solution;

2) The solvate may melt either congruently or incongruently;

3) Based on DTA experiments, the temperature of the eutectics ($pyridine_{(solid)}$ + $solvate_{(solid)}$ = liquor) was believed to be very close to the melting point of pure pyridine;

4) The behavior of the liquidus curve was taken to be as expected, i.e. not anomalous.

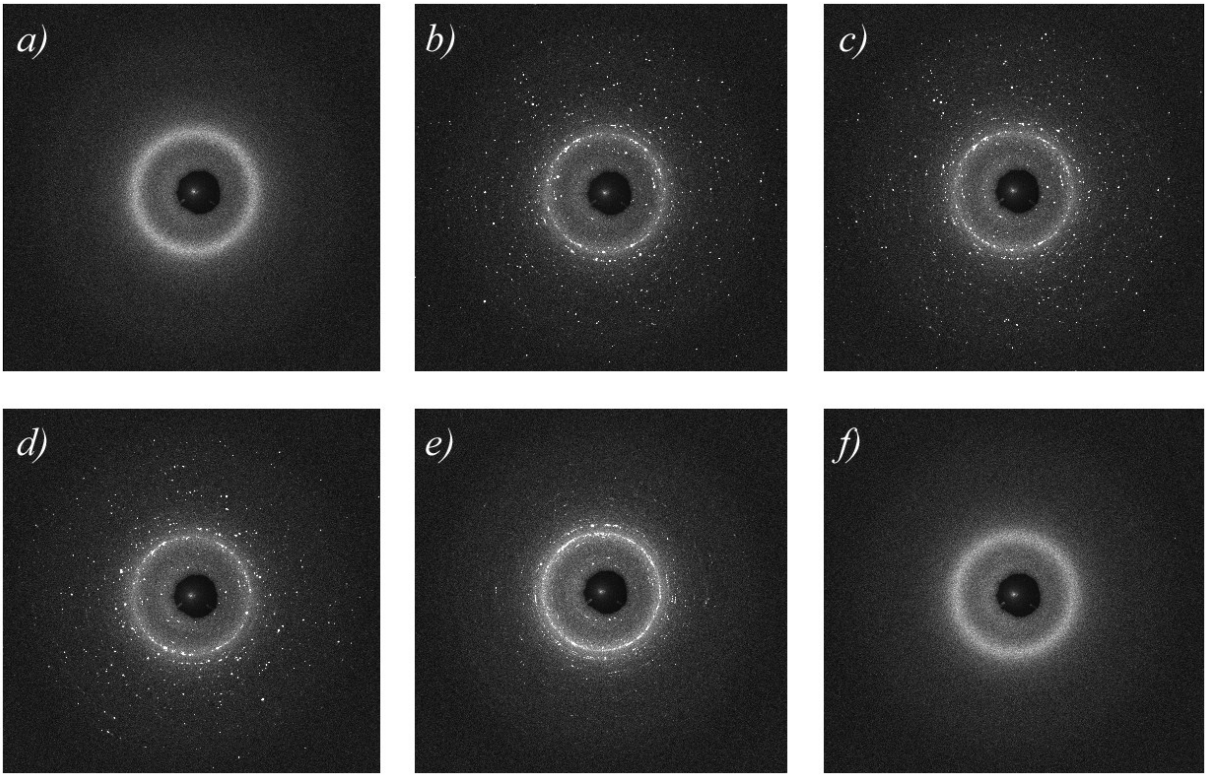

Figure S1. Two-dimensional X-ray diffraction patterns of paracetamol-pyridine quench-cooled solutions at different temperatures, illustrating formation of amorphous and crystalline phases in the system: a) 228 K, b) 243 K, c) 258 K, d) 268 K, e) 275 K, f) 277 K. See comments in the text

Different types of phase diagrams were compared with the experimental solubility and diffraction data, allowing selection of the correct type.

The possibility of congruent melting of the solvate, irrespectively to the solvate stoichiometry (Fig. S2, a) could be excluded based on diffraction experiments. In fact, although it was possible to build the liquidus curve to satisfy the results of the diffraction experiments, at least two compositions from the solubility test (two-phase region: paracetamol$_{(\text{solid phase})}$ + liquor) appeared on the phase diagram in the region which would correspond to a single-phase region, provided congruent melting occurred. These two compositions in the two-phase region (paracetamol$_{(\text{solid phase})}$ + liquor) would fall in the two-phase region "solid solvate + liquor", even if the solvate were assumed to melt at a higher temperature.

The model that assumes the solvate to be stable up to a certain temperature and then decompose in the solid state into the initial components of the system (i.e. the model assuming the solvate to be an "exothermic compound") (Fig. S2, d) also contradicts experimental data. Diffraction experiments have shown that the solvate$_{(\text{solid phase})}$ and liquor coexist in the region, where the co-existence of paracetamol$_{(\text{solid phase})}$ + liquor could be expected, should the model of "exothermic compound" be valid.

The only two models which are in complete agreement with experimental data are those assuming that the solvate melts incongruently, independently on whether the solvate is stable

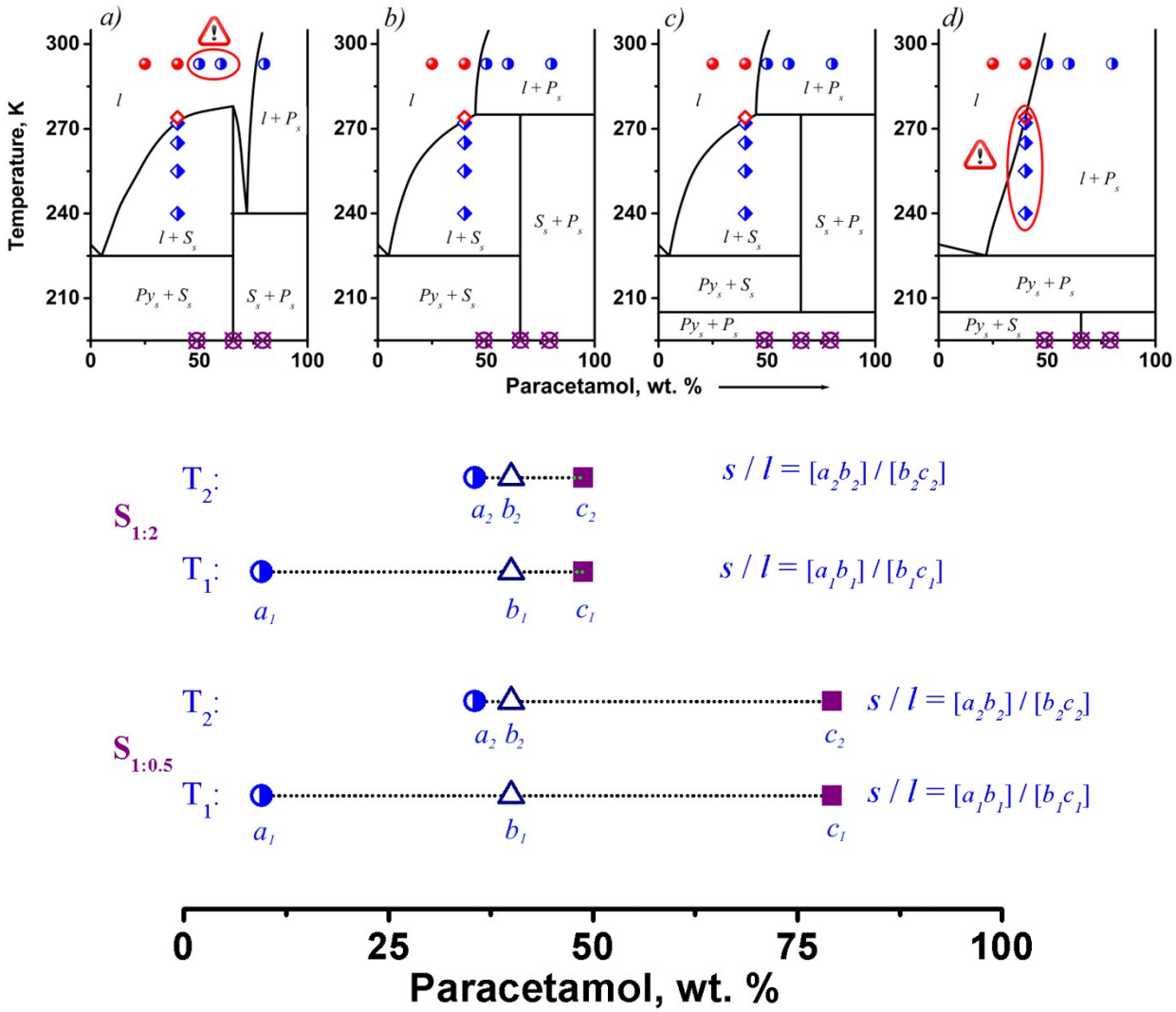

Figure S2. (above) Possible models of the "paracetamol-pyridine" phase diagram. Estimated compositions of paracetamol-pyridine solvate (1:2; 1:1; 1:0.5) shown as crossed purple circles. For clarity, in each case the model is presented for only one solvate composition. Designations: Py – pyridine; P – paracetamol; S – paracetamol – pyridine solvate; l – liquor; s – solid phase. Data on solubility of paracetamol in pyridine are shown as red circles (one-phase region: liquor) and half-filled blue circles (two-phase region: "paracetamol(solid phase) + liquor"). The results of diffraction experiments are shown as half-filled blue rhombuses (two-phase region: "solvate(solid phase) + liquid phase") and red rhombuses (one-phase region: liquor). Only variants b) and c) are consistent with the experimental data. More comments in the text.
(below) Examples of solvates with maximum (paracetamol : pyridine = 1:2, $S_{1:2}$) and minimum (pyridine : paracetamol = 1:2, $S_{1:0.5}$) pyridine content, with changes in the ratios of the liquid phase and resulting solvate crystals at different temperatures shown in real scale based on Fig. 1a. Designations: T_1 and T_2 – minimum and maximum allowed crystallisation temperature; liquid phase - half-filled blue circles; purple squares – solid phases of estimated paracetamol – pyridine solvates; blue triangle – position of state point

across the whole temperature range below the peritectic (Fig. S2, b), or within certain temperature boundaries (i.e. solvate is an "endothermic compound") (Fig. S2, c). The two-phase regions, "solid solvate + liquor," are the same for both models. Since the subsolidus region is of no interest for obtaining single crystals, for the sake of simplicity we considered only one variant (*b*) when searching for optimum concentration and temperature ranges for successful single

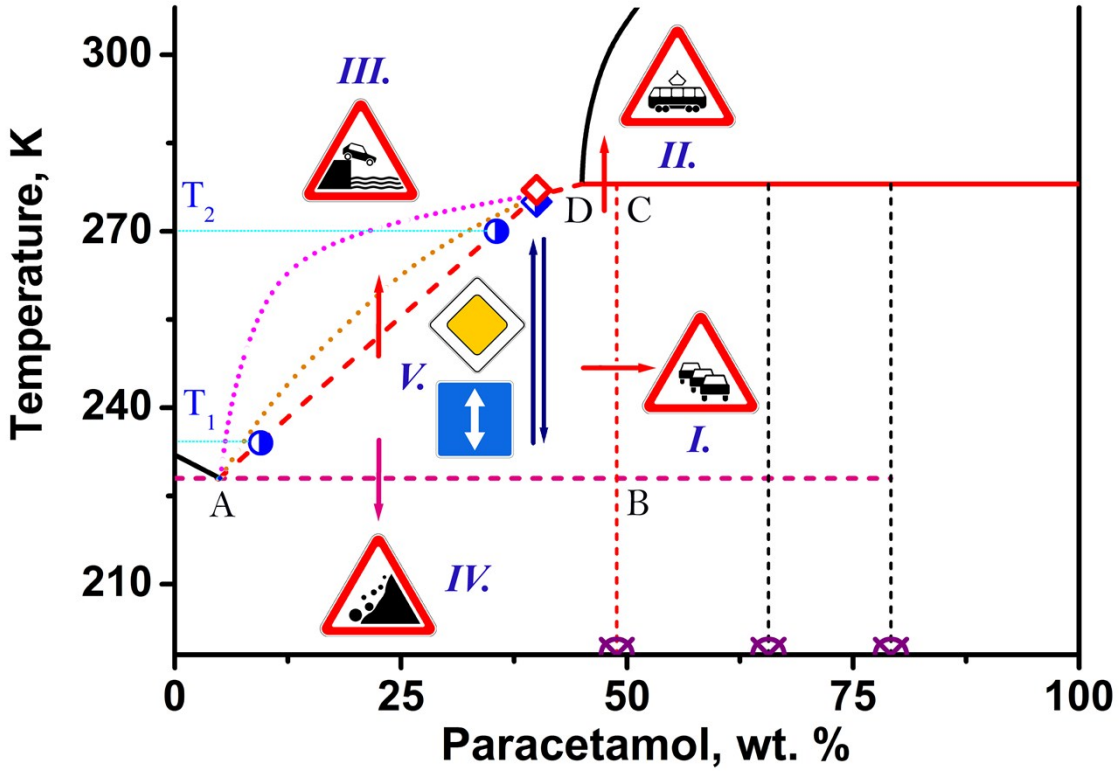

Figure S3. Selecting the conditions for obtaining the paracetamol-pyridine solvate crystal suitable for single-crystal X-ray diffraction. Comments are in the text (Part II)

crystal growth. The range in which crystallization is possible ("solid solvate – liquor" field at the phase diagram) is represented by a rectangular trapezoid ABCD (Fig. S3, and Fig. 1 in the main text).

The principle of selecting the conditions for obtaining the paracetamol-pyridine solvate crystal suitable for single-crystal X-ray diffraction is illustrated by Fig. S3. The results of the diffraction experiments around the liquidus curve are shown as a half-filled blue rhombus (two-phase region: "solvate(solid phase) + liquid phase") and a red rhombus (one-phase region: liquor). Road signs mark the regions that are unsuitable for the growth of solvate crystals: I. "Traffic queues likely ahead" means that there is no liquor now; finely dispersed phases of solvate and paracetamol will co-exist, and the growth of single crystals will stop because no material will be left. II. "Tram crossing ahead" means that one is in the stability region of solid paracetamol now; III. "Unprotected quayside or river bank" means that there is danger of losing polycrystals of the metastable phase by drowning (melting)); IV. "Falling rocks or debris" means that there is danger of spontaneous crystallization of monoclimic paracetamol; V. "Priority road" + "two way traffic" – the only possible way of obtaining a single crystals by performing a series of heating/cooling of quench-frozen sample.

Part III. Single-crystal diffraction experiment

Single-crystal X-ray diffraction at ambient and variable temperatures was studied using a STOE IPDS II diffractometer (*Mo Kα* radiation) with an Oxford Cryostream cooling device (temperature was maintained with a precision of 0.1 K). Data collection (ω-scan) and crystal structure refinement were carried out at 100, 125, 150, 175, 200, 225, 250, 275 K. The software used for data collection and cell refinement was X-AREA [S5], and that for data reduction was X-RED [S5]. The absorption of X-rays by the crystals was not taken into account since there are only light atoms in the structure (μ = 0.09 mm^{-1}). Since the crystal is not stable in air for the duration of the entire experiment, the crystal was covered by cryo-oil to avoid sample decomposition. The crystal structure at each temperature was solved by direct methods using SHELXS97 [S6] and refined using SHELXL97 [S6] with X-STEP32 as GUI [S7]. STRAIN [S8] was used to calculate the lattice strain anisotropy. A summary of the parameters characterizing data collection and refinement is given in Table S1. Mercury [S9] and Platon [S10] were used for structure visualization and analysis. EnCIFer [S11] and online IUCr services were used to prepare CIFs for publication. A summary of crystal data, data collection and data refinement parameters is given in Table S1. Complete structural data were deposited in the CSD [S12] with refcodes CCDC 816885 – 816892.

Crystal structure and the anisotropy of structural strain on cooling are discussed in the main text. Fig. S4 presents an overlay of two independent paracetamol molecules illustrating the difference in the torsion angle C7-N1-C4-C5. Table S2 summarizes the geometry parameters for hydrogen bonds, Fig. S5 shows the changes in the geometry parameters of hydrogen bonds on cooling. Table S3 and Fig. S6 contain data on the anisotropy of linear strain on cooling.

The values of relative compression for the three types of hydrogen bonds on cooling from 275 to 100 K were ~ -1.2% for N1A-H1A...O2B (-x, y+1/2, -z+1/2), ~-1.4% for N1B-H1B...O2A (-x, -y+1, -z), ~-0.5% for O1B-H11B...O1A (-x+1, y-1/2, -z+1/2) and ~-0.6% for O1A-H11A...N1S. No significant changes in molecular geometry (*i.e.* the angles C7-N1-C4-C5 for A and B molecules) were detected. Changes in the angles between the aromatic rings in two symmetrically independent paracetamol molecules and the pyridine ring were approximately 1.7º on cooling from 275 to 100 K. Changes in these angles contribute to the overall magnitude of compression along the axis of major compression (axis 3). As a benchmark example, all molecules are symmetry related in monoclinic paracetamol, and as such compression on cooling does not lead to changes in the relative orientation of paracetamol molecules. Compression of the intermolecular H-bonds in *bis*(paracetamol) pyridine accounts for a large amount of the linear strain on cooling. The structure is least compressible in the direction of the chains linked by OH…OH bonds (close to axis ***a***), whereas the direction of major compression (which must be normal to axes ***a*** and ***b*** by the formal symmetry requirements) is between the ***a*** and ***c*** axes.

Table S1. Experimental details for data collection and crystal structure refinement. For all structures: 2(C8H9NO2)·C5H5N, Mr = 381.42, monoclinic, $P2_1/c$, Z = 4, Crystal size (mm) 0.35 × 0.30 × 0.30. Experiments were carried out with Mo Kα radiation using a STOE IPDS II diffractometer. Refinement was on 281 parameters. H-atom parameters were constrained

Crystal data				
Temperature (K)	100	125	150	175
a, *b*, *c* (Å)	15.5127 (13), 8.2524 (5), 17.957 (2)	15.5180 (14), 8.2664 (5), 17.978 (2)	15.5225 (14), 8.2788 (5), 17.997 (2)	15.5304 (15), 8.2953 (6), 18.026 (2)
β (°)	122.004 (6)	121.982 (7)	121.964 (7)	121.942 (8)
V (Å^3)	1949.4 (3)	1956.1 (3)	1962.1 (3)	1970.7 (3)
D_x (Mg m^{-3})	1.300	1.295	1.291	1.286
No. of reflections for cell measurement	10933	10046	9208	8433
μ (mm^{-1})	0.09	0.09	0.09	0.09
Data collection				
No. of measured, independent and observed [$I > 2\sigma(I)$] reflections	18297, 5247, 3690	18352, 5267, 3547	18407, 5289, 3404	18493, 5314, 3219
R_{int}	0.046	0.045	0.047	0.048
$(\sin\theta/\lambda)_{max}$ (Å^{-1})	0.686	0.686	0.686	0.686
Range of *h*, *k*, *l*	*h* = -21→21, *k* = -11→11, *l*= -24→24	*h* = -21→20, *k* = -11→11, *l*= -24→24	*h* = -21→20, *k* = -11→11, *l*= -24→24	*h* = -21→20, *k* = -11→11, *l*= -24→24
Refinement				
$R[F^2 > 2\sigma(F^2)]$, $wR(F^2)$, *S*	0.040, 0.095, 1.00	0.040, 0.093, 0.98	0.041, 0.092, 0.94	0.041, 0.096, 0.92
No. of reflections	5247	5267	5289	5314
$\Delta\rho_{max}$, $\Delta\rho_{min}$ (e Å^{-3})	0.24, -0.22	0.24, -0.22	0.20, -0.18	0.19, -0.18
Crystal data				
Temperature (K)	200	225	250	275
a, *b*, *c* (Å)	15.5367 (16), 8.3081 (6), 18.051 (2)	15.5427 (16), 8.3248 (6), 18.084 (2)	15.5486 (17), 8.3370 (7), 18.116 (3)	15.5533 (18), 8.3475 (7), 18.151 (3)
β (°)	121.906 (8)	121.851 (8)	121.807 (8)	121.742 (9)
V (Å^3)	1978.0 (4)	1987.6 (4)	1995.7 (4)	2004.1 (4)
D_x (Mg m^{-3})	1.281	1.275	1.269	1.264
No. of reflections for cell measurement	7780	7347	6744	6367
μ (mm^{-1})	0.09	0.09	0.09	0.09
Data collection				
No. of measured, independent and observed [$I > 2\sigma(I)$] reflections	18597, 5341, 3081	18685, 5363, 2915	18770, 5386, 2702	18870, 5416, 2570
R_{int}	0.050	0.050	0.053	0.052
$(\sin\theta/\lambda)_{max}$ (Å^{-1})	0.686	0.687	0.686	0.686
Range of *h*, *k*, *l*	*h* = -21→20, *k* = -11→11, *l*= -24→24	*h* = -21→20, *k* = -11→11, *l*= -24→24	*h* = -21→20, *k* = -11→11, *l*= -24→24	*h* = -21→20, *k* = -11→11, *l*= -24→24
Refinement				
$R[F^2 > 2\sigma(F^2)]$, $wR(F^2)$, *S*	0.043, 0.095, 0.89	0.043, 0.098, 0.89	0.043, 0.101, 0.86	0.045, 0.108, 0.87
No. of reflections	5341	5363	5386	5416
$\Delta\rho_{max}$, $\Delta\rho_{min}$ (e Å^{-3})	0.17, -0.17	0.17, -0.14	0.16, -0.14	0.16, -0.14

Table S2. Selected hydrogen-bond parameters at different temperatures. Symmetry code(s): (i) -x, y+1/2, -z+1/2; (ii) -x, -y+1, -z; (iii) -x+1, y-1/2, -z+1/2; atoms designations as at Figure 2 (main text)

D—H···*A*	*D*—H (Å)	H···*A* (Å)	*D*···*A* (Å)	*D*—H···*A* (°)
100 K				
N1A—H1A···O2B^{i}	0.88	1.97	2.8415 (14)	172.4
N1B—H1B···O2A^{ii}	0.88	1.96	2.8331 (13)	170.7
O1B—H11B···O1A^{iii}	0.84	1.90	2.7357 (13)	170.7
O1A—H11A···N1S	0.84	1.83	2.6512 (14)	166.7
125 K				
N1A—H1A···O2B^{i}	0.88	1.97	2.8464 (14)	172.2
N1B—H1B···O2A^{ii}	0.88	1.97	2.8408 (14)	170.8
O1B—H11B···O1A^{iii}	0.84	1.90	2.7362 (13)	170.6
O1A—H11A···N1S	0.84	1.83	2.6532 (15)	166.7
150 K				
N1A—H1A···O2B^{i}	0.88	1.98	2.8504 (14)	172.1
N1B—H1B···O2A^{ii}	0.88	1.97	2.8444 (14)	170.9
O1B—H11B···O1A^{iii}	0.84	1.91	2.7384 (14)	170.3
O1A—H11A···N1S	0.84	1.83	2.6540 (15)	167.8
175 K				
N1A—H1A···O2B^{i}	0.88	1.98	2.8569 (15)	172.1
N1B—H1B···O2A^{ii}	0.88	1.98	2.8506 (15)	171.0
O1B—H11B···O1A^{iii}	0.84	1.91	2.7412 (15)	169.6
O1A—H11A···N1S	0.84	1.83	2.6580 (16)	167.9
200 K				
N1A—H1A···O2B^{i}	0.88	1.99	2.8610 (15)	172.4
N1B—H1B···O2A^{ii}	0.88	1.98	2.8540 (16)	171.2
O1B—H11B···O1A^{iii}	0.84	1.91	2.7399 (16)	169.7
O1A—H11A···N1S	0.84	1.83	2.6603 (17)	167.5
225 K				
N1A—H1A···O2B^{i}	0.87	2.00	2.8667 (16)	172.5
N1B—H1B···O2A^{ii}	0.87	2.00	2.8639 (16)	171.4
O1B—H11B···O1A^{iii}	0.83	1.92	2.7430 (17)	170.4
O1A—H11A···N1S	0.83	1.85	2.6639 (18)	167.7
250 K				
N1A—H1A···O2B^{i}	0.87	2.00	2.8693 (17)	172.6
N1B—H1B···O2A^{ii}	0.87	2.01	2.8685 (17)	171.4
O1B—H11B···O1A^{iii}	0.83	1.93	2.7466 (18)	169.3
O1A—H11A···N1S	0.83	1.84	2.6616 (19)	169.3
275 K				
N1A—H1A···O2B^{i}	0.86	2.02	2.8770 (18)	172.9
N1B—H1B···O2A^{ii}	0.86	2.02	2.8733 (19)	171.6
O1B—H11B···O1A^{iii}	0.82	1.94	2.7483 (19)	169.2
O1A—H11A···N1S	0.82	1.85	2.666 (2)	170.8

Table S3. Parameters characterizing linear strain along the principal axes of strain ellipsoid for bis(paracetamol) pyridine on cooling

Angle (°) with			
	A (error)	B (error)	C (error)
Axis 1	1.6(0.3)	90(0)	120.1(0.3)
Axis 2	90(0)	0(0)	90(0)
Axis 3	91.6(0.3)	90(0)	30.1(0.3)

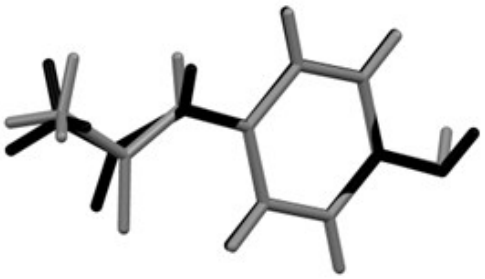

Figure S4. Overlay of paracetamol molecules with different conformations in bis(paracetamol) pyridine

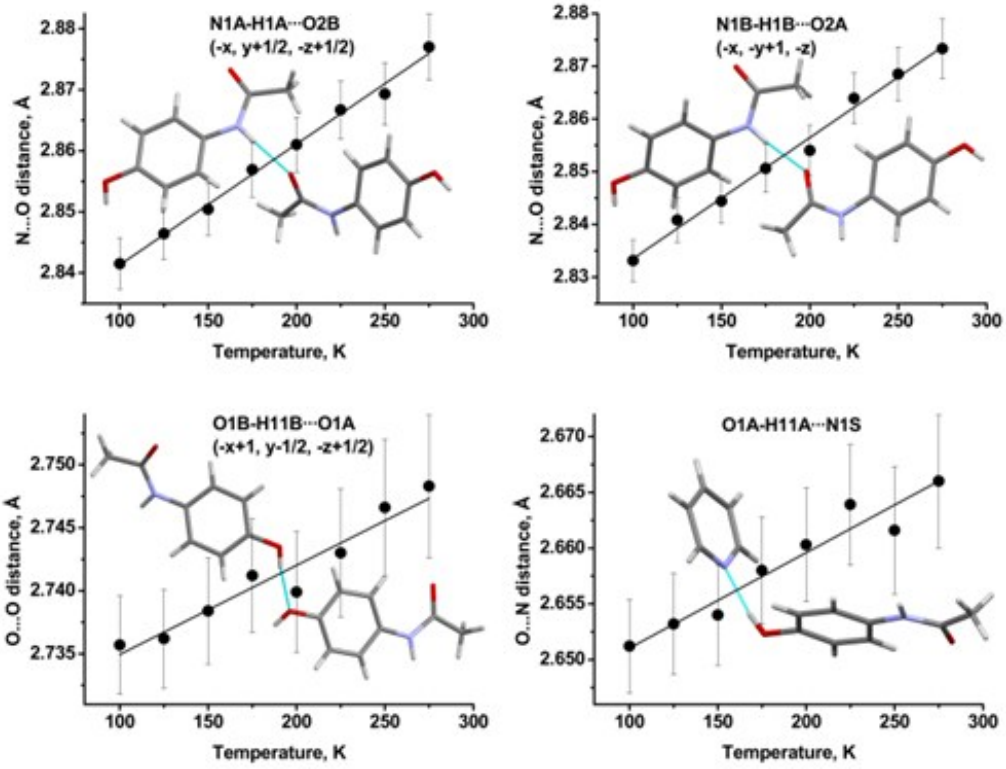

Figure S5. The distances between non-hydrogen atoms in hydrogen bonds *vs*. temperature

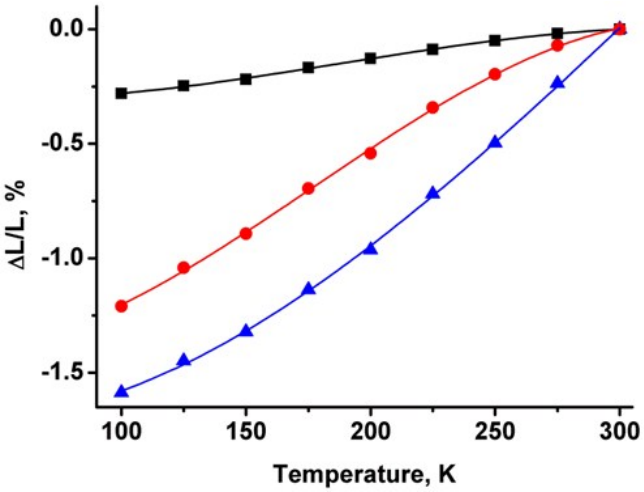

Figure S6. Linear strain in the directions of the principal axes of the strain ellipsoid versus temperature in *bis*(paracetamol) pyridine. The values of linear strain along the principal axes of the strain tensor [1 - minimum linear size of strain ellipsoid, 2 - normal to 1 and 3, 3 - maximum linear size of strain ellipsoid] are plotted as squares, circles and triangles, respectively. The curves are extrapolated to ambient temperature, which is taken as a reference point

Unfortunately, it is not possible to compare the anisotropy of strain on cooling in *bis*(paracetamol) pyridine with that for other multicomponent paracetamol crystals, since no variable-temperature data were reported for the latter. Individual paracetamol polymorphs [S13, S14], were more compressible in the direction close to the N-H...O hydrogen bonds, whereas there was no significant compression in the direction of O-H...O hydrogen bonds. In this respect behaviour of *bis*(paracetamol) pyridine is similar to that of the pure polymorphs of paracetamol on cooling. At the same time the maximum compression of pure paracetamol was observed perpendicular to the paracetamol layers for both polymorphs, a different trend from *bis*(paracetamol) pyridine. In monoclinic and orthorhombic paracetamol all molecules are symmetry-related, and compression along the band axes are related to changes in intermolecular hydrogen bonds, but not to the changing of paracetamol orientation within the layers.

References

S1 N. V Surovtsev, S. V Adichtchev, V. K. Malinovsky, A. G. Ogienko, V. A. Drebushchak, A. Y. Manakov, A. I. Ancharov, A. S. Yunoshev and E. V Boldyreva, *J. Chem. Phys.*, 2012, **137**, 065103.

S2 A. I. Ancharov, A. Y. Manakov, N. A. Mezentsev, B. P. Tolochko, M. A. Sheromov and V. M. Tsukanov, *Nucl. Instruments Methods Phys. Res. Sect. A Accel. Spectrometers, Detect. Assoc. Equip.*, 2001, **470**, 80–83.

S3 A. G. Ogienko, A. V Kurnosov, A. Y. Manakov, E. G. Larionov, A. I. Ancharov, M. A. Sheromov and A. N. Nesterov, *J. Phys. Chem. B*, 2006, **110**, 2840–2846.

S4 A. P. Hammersley, *Eur. Synchrotron Res. Facil. Grenoble, Fr. 2003*, 2003.

S5 Stoe and Cie, 2007, X-AREA and X-RED32, Stoe and Cie, Darmstadt, Germany.

S6 G. M. Sheldrick, *Acta Crystallogr. A.*, 2008, **64**, 112–122.

S7 Stoe and Cie, 2000, X-STEP32, Stoe and Cie, Darmstadt, Germany.

S8 Y. Ohashi and C. W. Burnham, *Am. Miner.*, 1973, **58**, 843–849.

S9 C. F. Macrae, P. R. Edgington, P. McCabe, E. Pidcock, G. P. Shields, R. Taylor, M. Towler and J. van de Streek, *J. Appl. Crystallogr.*, 2006, **39**, 453–457.

S10 A. L. Spek, *J. Appl. Crystallogr.*, 2003, **36**, 7–13.

S11 F. H. Allen, O. Johnson, G. P. Shields, B. R. Smith and M. Towler, *J. Appl. Crystallogr.*, 2004, **37**, 335–338.

S12 F. H. Allen, *Acta Crystallogr. Sect. B Struct. Sci.*, 2002, **58**, 380–388.

S13 T. N. Drebushchak and E. V. Boldyreva, *Z. Krist.*, 2004, **219**, 506–512.

S14 C. C. Wilson, *Z. Krist.*, 2000, **215**, 693–701.